Soils and Foundations 2013;53(3):395–407

The Japanese Geotechnical Society

Soils and Foundations

www.sciencedirect.com
journal homepage: www.elsevier.com/locate/sandf

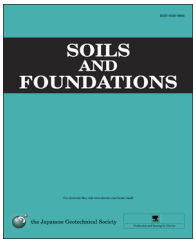

Numerical evaluation of effects of nonlinear lateral pile vibrations on nonlinear axial response of pile shaft

Malek Allani, Alain Holeyman*

Université Catholique de Louvain (UCL), Louvain-la-Neuve, Belgium

Received 17 October 2011; received in revised form 5 February 2013; accepted 21 February 2013
Available online 17 May 2013

Abstract

Axial and lateral dynamic pile analyses are generally handled separately; and consequently, dynamic soil reactions are assumed to be uncoupled. However, pure loading is rarely encountered as combined loading occurs in many situations (offshore piles, pile driving as well as pile groups and pile rafts). In this study, the effects of nonlinear lateral pile vibrations on the in-phase nonlinear axial pile response of a pile shaft are studied. New approximate nonlinear solutions for both axial and lateral pile behavior, developed from general elastodynamic equations, are presented. The solutions are obtained by extending the elastodynamic solution for plane strain cases with a view to model soil nonlinearity. Since axial soil resistance depends on the confining stress around the pile shaft, the effect of the lateral soil behavior on the confining pressure of the pile circumference is investigated and the axial soil reaction from coupled in-phase vibrations is derived. It is concluded that the axial unit shear strength significantly increases when lateral soil vibrations involve plasticity, which in turn results in an increase in the axial dynamic resistance of the pile shaft.

JEL Classifications: IGC: D07; E03; E12

Keywords: Axial & lateral soil vibration; Nonlinear dynamic analysis; Coupling impedance

1. Introduction

Pile vibration analyses have been widely treated in literature with the Winkler approach being a commonly used method for calculating pile response under either axial or lateral vibration modes. Following the Winkler approach, the soil can be replaced by an infinite series of independent springs and dashpots, providing either axial or lateral soil resistance. Soils exhibit a strongly nonlinear behavior, especially under high strain loading situations (offshore piles, windmill foundations and so on) either in lateral or axial loading modes. The seismic loading of pile groups and piled rafts also induces combined lateral and axial dynamic loads on individual piles. A number of shear modulus versus shear strain relationships have been developed in literature to handle such nonlinearity. Among them, the hyperbolic model by Kondner (1963), the empirical stress–strain relationship by Ishibashi and Zhang (1993) and the experimental curves by Vucetic and Dobry (1991) have gained some popularity among geotechnical engineers (Ishihara, 1996; Kramer, 1996).

Novak's solution can be considered as the reference viscoelastic solution for axial soil vibrations using elasto-dynamic equations (Novak, 1974, 1977; Novak et al., 1978). The solution was derived by assuming a plane strain condition in the horizontal soil layers surrounding a pile shaft, without

*Corresponding author. Tel:+3210472112; fax: +3210472179.
E-mail addresses: malek.allani@uclouvain.be (M. Allani), alain.holeyman@uclouvain.be (A. Holeyman).
Peer review under responsibility of The Japanese Geotechnical Society.

Production and hosting by Elsevier

0038-0806
http://dx.doi.org/10.1016/j.sandf.2013.04.002

taking soil degradation into account. Novak and Sheta (1980) and Mitwally and Novak (1988) proposed a more realistic soil response model able to account for the plastic zone around the pile shaft. They suggested distinguishing two separate radial soil zones around the pile, namely, an inner zone with reduced shear stiffness and an outer zone where the elastic solution is considered. According to Novak et al. (1978), the elastic soil reaction is considered in the far field, since deformations are small enough. Han and Sabin (1995) solved the nonlinear axial soil vibration problem by considering an inner zone where properties gradually reach those of the outer zone using a parabolic variation for the shear modulus. El Naggar and Novak, 1994a, 1994b) adopted the same approach, implementing the hyperbolic Kondner (1963) stress–strain relationship in the inner zone. Michaelides and Gazetas (1995), Michaelides et al. (1997, 1998) developed semi-analytical solutions for given radially inhomogeneous shear modulus distributions, based on the experimental studies of Seed and Idriss (1970), Richart et al. (1970), and Vucetic and Dobry (1991).

Nogami and Novak (1977) elaborated a rather general solution (including depth-dependence) to derive the lateral soil reaction from an elastodynamic equation. The solution of Novak et al. (1978) constitutes a particular case for the solution of Nogami and Novak (1977), since it is based on plane strain conditions. The lateral model suggested by El Naggar and Novak (1995, 1996), to account for nonlinear soil behavior, is also based on the Winkler approach. The nonlinear stiffness is calculated according to the strain level where ultimate soil resistance was estimated according to American Petroleum Institute (API, 1991) standards. Chau and Yang (2005) also developed a nonlinear model for horizontally vibrating piles. Their work is an extension of the model suggested by Nogami and Novak (1977) incorporating the depth-dependency of the lateral soil displacement. Even though the solution by Nogami and Novak (1977) is more rigorous than the plane strain solution, its major drawback is the inability to handle horizontally heterogeneous soil layers.

All the above-mentioned studies focused on either axial or lateral pile vibrations. It was felt by the authors, therefore, that the coupling of the two vibration modes would be of original interest. Thus, a significant difficulty is added to the dynamic pile behavior, namely, the complex combination of axial and bending (lateral) vibration modes. In fact, Poskitt, 1992, 1991) and Holeyman (1992) attest that not only compressive waves, but also flexural oscillation and pile whipping can be generated in many situations, according to field observations where extreme conditions may be reached, such as offshore piles (Nishimura et al., 2012), windmill pile foundations, pile raft foundations (Vrettos and Borchrt, 2011) and so on. Using centrifuge and shaking table tests performed on piled rafts models, Horikoshi et al. (2003) and Matsumoto et al. (2004) experimentally demonstrated that even under horizontal shaking alone, axial loads as well as horizontal loads are caused in the piles, and that the same loading frequency can be found in both horizontal and vertical directions.

Fig. 1 presents a general situation (windmill pile) in which a pile, embedded in independent horizontal layers, is simultaneously loaded axially and laterally. Thus, the soil is loaded under both lateral and axial directions at each contact level with the pile shaft. The objective of this paper is to investigate the gain (or eventual loss) of the axial soil impedance (or resistance) due to the lateral loading at a given horizontal layer (Fig. 1).

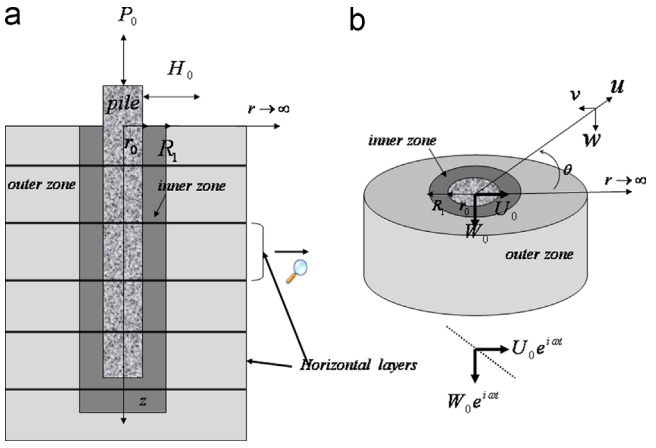

Fig. 1. (a) Pile subjected to axial and lateral harmonic load embedded into independent horizontal layers and (b) applied in-phase axial and lateral pile displacements within the considered horizontal layer.

All soil impedance expressions in this paper have been developed assuming plane strain conditions. Firstly, the nonlinear soil impedance (stiffness and dashpots) against axial and lateral vibrations, an extension of the work of Novak et al. (1978), is presented. Then, the effects of the dynamic nonlinear lateral soil reaction on the axial soil impedance through the computed mean radial stress are investigated. The dynamic lateral pile displacement is considered in this paper to be in phase with the axial soil displacement, as shown in Fig. 1. Finally, coupled axial soil impedances are presented under both common and extreme loading situations.

2. Nonlinear stress strain relationships

Since a nonlinear analysis is considered in this paper, for either axial or lateral pile vibrations, the available stress–strain relationships will be reviewed. One of the conventional ways of representing the soil nonlinear shear response in literature is the hyperbolic model, where degraded secant shear modulus G is expressed as (Kondner, 1963; Hardin and Drnevich, 1972; Hardin, 1978)

$$G = \frac{\tau_{max}}{\gamma_{ref} + \gamma} \tag{1}$$

where τ_{max} is the maximum shear stress (shear strength), γ is the shear strain and γ_{ref} is the reference shear strain defined as

$$\gamma_{ref} = \frac{\tau_{max}}{G_{max}} \tag{2}$$

with G_{max} being the initial shear modulus.

Hysteretic damping coefficient ξ can be defined as

$$\xi = \frac{\Delta E}{4\pi E_e} \tag{3.a}$$

expressing the energy lost ΔE in a cycle of amplitude γ_c relative to restorable (elastic) energy $E_e = ((1/2)G_{max}\gamma_C^2)$.

Hysteretic damping ξ corresponds to the hyperbolic law and can be expressed as

$$\xi = \frac{2}{\pi}\left(2\frac{\gamma_{ref}}{\gamma_c^2}(\gamma_c+\gamma_{ref})ln\left(\frac{\gamma_{ref}}{\gamma_c+\gamma_{ref}}\right)+2\frac{\gamma_{ref}}{\gamma_c^2}+1\right) \quad (3.b)$$

The main advantages of the hyperbolic model are its simplicity of implementation and its smooth transition from linear to perfectly plastic behavior. The hyperbolic curve has a slope G_{max} at γ=0 and smoothly reaches an asymptotic plateau of $\tau = \tau_{max}$ for γ=∞, while secant slope G continuously decreases as γ increases. Hardin and Drnevich (1972), Hardin (1978) and Richart et al. (1970), found that by representing the data in the normalized form, τ/τ_{max} vs γ/γ_{ref}, curves from various clay and sand specimens could be consolidated into a single, adjusted hyperbola.

An alternate stress–strain relation has also been considered in this paper, namely, the empirical relation suggested by Ishibashi and Zhang (1993), in which the degradation of the shear modulus is expressed as a function of shear strain γ, of confining mean stress σ' and of plasticity index IP.

$$\frac{G}{G_{max}} = 0.5\left\{1+tan\,h\left(0.492\,ln\frac{0.000102+n}{\gamma}\right)\right\}\sigma'^{m} \quad (4.a)$$

where

$$m = 0.272\left\{1-tanh\left(0.4\,ln\frac{0.000556}{\gamma}\right)\right\}e^{-0.0145IP^{1.3}} \quad (4.b)$$

$$n = \begin{cases} 0.0 & \text{for} \quad IP = 0 \\ 3.37\times10^{-6}IP^{1.404} & \text{for} \quad 0 < IP \le 15 \\ 7\times10^{-7}IP^{1.976} & \text{for} \quad 15 < IP \le 70 \\ 2.7\times10^{-5}IP^{1.115} & \text{for} \quad IP > 70 \end{cases} \quad (4.c)$$

and

$$\sigma' = \frac{\sigma_1' + \sigma_2' + \sigma_3'}{3} \quad (4.d)$$

where σ_1', σ_2' and σ_3' are the principal effective stress levels.

The hysteretic damping coefficient resulting from Eqs. (3.a), (4.a), (4.b) and (4.c) can be expressed as (Ishibashi and Zhang, 1993)

$$\xi = \frac{1+e^{-0.0145IP^{1.3}}}{6}\left[0.586\left(\frac{G}{G_{max}}\right)^2 - 1.547\frac{G}{G_{max}} + 1\right] \quad (5)$$

Even though the relationship by Ishibashi and Zhang (1993) is qualitatively similar to the experimental curves of Vucetic and Dobry (1991), the major difference results from the effects of confining stress σ' on the degraded law, which is limited to sandy soils and which can be disregarded for high plasticity soils (Michaelides et al., 1998).

The relations of both Kondner (1963) and Ishibashi and Zhang (1993) will be used in this paper to derive the nonlinear pile shaft response under axial as well as lateral vibrations. Fig. 2a and b compare the shear modulus and the hysteretic damping evolutions, respectively, as functions of shear strain. Higher soil degradation is observed for a lower plasticity index for the Ishibashi and Zhang (1993) relation and for a lower strain reference of γ_{ref} for the hyperbolic relation.

Fig. 2b also clearly indicates that the hysteretic damping coefficient reaches an asymptotic value of $(2/\pi)$ for any value of reference strain for the hyperbolic law. For Ishibashi and Zhang's law, the asymptotic value of ξ depends on plasticity index $(\xi_{IP}^{max} = ((1+e^{-0.0145IP^{1.3}})/6)$ reaching a maximum of 33% for IP=0 and 18.3% for IP=50.

It is also interesting to note that the shear modulus degradation law of Ishibashi for IP=0 is close to that of Kondner for γ_{ref} of about 3×10^{-4}.

For the numerical analysis discussed herein, the initial (or maximum) shear modulus can be calculated using the relation by Richart and Wylie (1978) and Woods and Wylie (1978), namely,

$$G_{max} = 6906\frac{(2.17-e)^2}{1+e}\sigma'^{0.5}[\text{kPa}] \quad (6)$$

where e is the void ratio and σ' is the initial effective confining stress calculated as

$$\sigma' = \frac{\sigma_v' + 2\sigma_{r,0}'}{3} \quad (7)$$

where σ_v' is the calculated effective initial vertical stress and $\sigma_{r,0}' = k\sigma_v'$ is the effective horizontal stress, with k being the

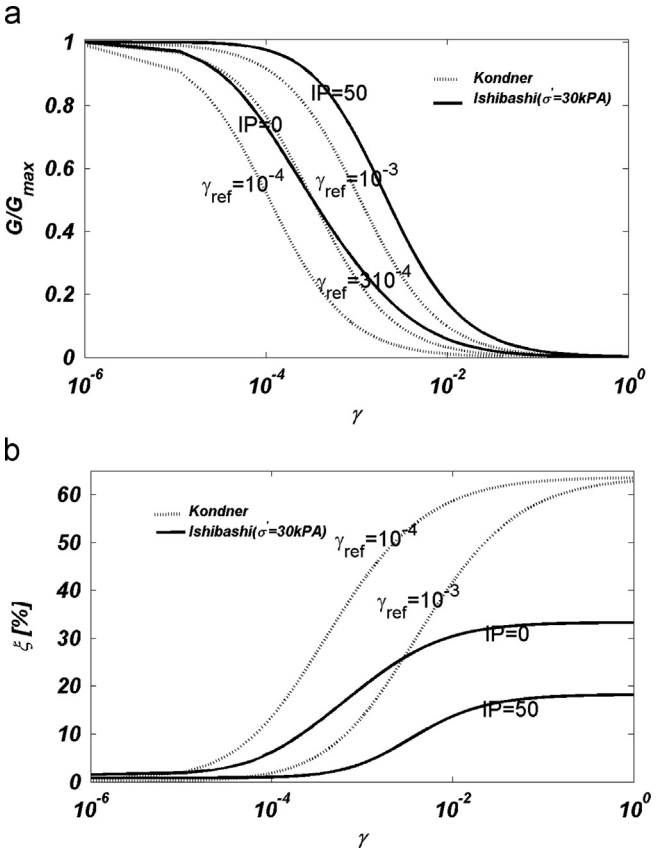

Fig. 2. Comparison of Kondner and Ishibashi and Zhang constitutive relationships: (a) nonlinear shear modulus-shear strain relationship and (b) hysteretic damping-shear strain relationship.

coefficient of horizontal stress for the soil at rest, calculated herein with Jacky's formula $k = 1-sin\varphi'$, wherein φ' is the internal friction angle.

Once the maximum shear modulus has been calculated, the unit shear strength (for both axial and lateral analyses) for the pile shaft is calculated by the Mohr–Coulomb criteria (for cohesionless soil).

$$\tau_{max} = \sigma'_{r,0} tan\ \delta \tag{8}$$

where δ is the interface friction angle. In general, δ depends on the roughness of the structure, internal friction angle φ' and mean particle size d_{50} (Jardine et al., 1992). Brumund and Leonerds (1973), Bolton (1991) and many other authors state that δ could be equal to φ' for the concrete–soil interface and for cast-in-place piles. Jardine et al. (1992, 2005), Jardine and Standing (2012)) and Tsuha et al. (2012) indicated that δ is within the range of 26° to 33° depending on d_{50}.

Consequently, reference stress–strain relation $\gamma_{ref} = (\tau_{max}/G_{max})$ can be deduced.

Two regions are considered to model the nonlinear soil response. An inner nonlinear viscoleastic zone in the shape of a hollow cylindrical tube, with an inner radius equal to pile radius r_0 and an outer radius equal to $R_1 > r_0$, is considered. Then, an outer viscoelastic infinite region is considered within radial coordinate r with $R_1 < r < \infty$ (Fig. 1).

3. Nonlinear visco-elastic axial soil resistance

3.1. General

The governing equation of axis-symmetric motion for pure dynamic vertical shear stress in homogenous elastic media is expressed as

$$\frac{\partial(r\tau_{rz})}{r\partial r} = \rho\frac{\partial^2 w}{\partial t^2} \tag{9}$$

where ρ is the soil density, w is the vertical soil displacement and τ_{rz} is the axial shear stress.

The general shear stress–shear strain elastic relation, applicable to the soil's axial shear, is expressed as

$$\tau_{rz} = G_{rz}\frac{\partial w}{\partial r} \tag{10}$$

where G_{rz} is the soil axial shear modulus.

3.2. Inner zone

By substituting Eq. (10) into Eq. (9), and since two regions are considered (Fig. 1), the displacement solution for the inner zone is that of a hollow cylinder. Assuming that the inner hollow cylinder is made of a visco-elastic medium, the displacement can be expressed by (Abramowitz and Stegum, 1972)

$$w = AK_0(\tfrac{\lambda}{r_0}r) + BI_0(\tfrac{\lambda}{r_0}r) \quad \text{With} \quad r_0 \le r \le R_1 \tag{11}$$

where A and B are constants depending on the boundary conditions, K_0 and I_0 are modified Bessel functions of the zero order of the first and second kind, respectively, and λ is expressed as

$$\lambda = \frac{ai}{\sqrt{1+i2\xi_{ax}}} \tag{12}$$

where $i = \sqrt{-1}$, ξ_{ax} is the equivalent axial hysteretic damping coefficient of the inner zone, and $a = (\omega r_0/V_s)$ is the dimensionless frequency of the inner zone where ω is the angular frequency and $V_s = \sqrt{(G_{rz}/\rho)}$ is the shear wave velocity of the inner zone.

3.3. Outer zone

In the outer zone, assumed to consist of another homogeneous visco-elastic medium, the solution by Novak et al., (1978) for the plane strain case is used. The displacement solution is expressed as

$$w = CK_0\left(\frac{\lambda_{max}}{R_1}r\right) \quad \text{With} \quad r \ge R_1 \tag{13}$$

where C is a constant, depending on the boundary conditions, and λ_{max} is expressed as

$$\lambda_{max} = \frac{a_{max}i}{\sqrt{1+i2\xi_{ax,min}}} \tag{14}$$

where $\xi_{ax,min}$ is the axial hysteretic damping coefficient of the outer zone, $a_{max} = (\omega r_0/V_{s_{max}})$ is the dimensionless frequency of the outer zone and $V_{s_{max}} = \sqrt{(G_{rz,max}/\rho)}$ is the shear wave velocity of the outer zone with $G_{rz,max}$ being the soil axial shear modulus of the outer zone. Solution (13) postulates a radiation condition at $r = \infty$ (Sommerfeld boundary condition).

3.4. Equivalent properties

An equivalent linearization technique is used to calculate the degraded shear modulus and the hysteretic damping within the inner zone. In fact, average axial strain $\overline{\gamma}_{rz}$ is defined in both stress–strain relationships to calculate the equivalent secant modulus G_{rz} and hysteretic damping ξ_{ax}. The expression for $\overline{\gamma}_{rz}$ is

$$\overline{\gamma}_{rz} = \frac{1}{(R_1-r_0)}\int_{r_0}^{R_1}|\gamma_{rz}|dr = \frac{1}{(R_1-r_0)}\int_{r_0}^{R_1}\left|\frac{\partial w}{\partial r}\right|dr \tag{15}$$

An iterative procedure is used for the calculation of consistent G_{rz} and ξ_{ax} values applicable to the inner zone. More specifically, initial elastic modulus $G_{rz,max}$ and hysteretic damping $\xi_{ax,min}$ are considered, and soil displacement is calculated using Eqs. (11) and (13). Then, the average strain calculated from Eq. (15) is substituted into Eqs. (1)–(5) to better assess degraded shear modulus G_{rz} and hysteretic damping ξ_{ax}. These updated values are used to complete a new equivalent visco-elastic analysis using Eqs. (11) and (13) to derive a new average shear strain, $\overline{\gamma}_{rz}$, from Eq. (15). Once again, Eqs. (1)–(5) are used to derive new G_{rz} and ξ_{ax} values. This iterative procedure is repeated until the convergence of $\overline{\gamma}_{rz}$, G_{rz} and ξ_{ax} has been achieved.

3.5. Matrix formulation

Constants A, B (Eq. (11)) and C (Eq. (13)) are determined by considering the following conditions:

1. Enforcing displacement $W_0e^{i\omega t}$ at the pile–soil interface
2. Continuity of displacement w across the two regions
3. Continuity of the shear stress τ_{rz} across the two regions.

These conditions lead to three simultaneous equations which can be written in matrix form as

$$[A_{ij}]_{3\times3}\Lambda = W \tag{16}$$

where

$$\Lambda = \begin{bmatrix} A & B & C \end{bmatrix}^T \tag{17}$$

$$W = \begin{bmatrix} W_0 & 0 & 0 \end{bmatrix}^T \tag{18}$$

where W_0 is the axial displacement applied at the pile–soil interface.

The matrix elements $[A_{ij}]_{3\times3}$ are expressed in Appendix A.

4. Nonlinear visco-elastic lateral soil resistance

4.1. General

The dynamic stress equilibrium equations under horizontal plane strain conditions are expressed in terms of radial and tangential displacements (u and v) as

$$\frac{1}{r}\frac{\partial(r\sigma_r)}{\partial r} + \frac{1}{r}\frac{\partial\tau_{r\theta}}{\partial\theta} - \frac{\sigma_\theta}{r} = \rho\frac{\partial^2 u}{\partial t^2} \tag{19}$$

$$\frac{\partial(r^2\tau_{r\theta})}{\partial r} + \frac{1}{r}\frac{\partial\sigma_\theta}{\partial\theta} = \rho\frac{\partial^2 v}{\partial t^2} \tag{20}$$

where r is the radial distance, θ is the circumferential angle and σ_r, σ_θ and $\tau_{r\theta}$ are the radial, tangential and shear stress, respectively. These stress levels are expressed as

$$\sigma_r = \lambda\left(\frac{\partial u}{\partial r} + \frac{u}{r} + \frac{1}{r}\frac{\partial v}{\partial\theta}\right) + 2G_{r\theta}\frac{\partial u}{\partial r} \tag{21}$$

$$\sigma_\theta = \lambda\left(\frac{\partial u}{\partial r} + \frac{u}{r} + \frac{1}{r}\frac{\partial v}{\partial\theta}\right) + 2G_{r\theta}\left(\frac{u}{r} + \frac{1}{r}\frac{\partial v}{\partial\theta}\right) \tag{22}$$

$$\tau_{r\theta} = G_{r\theta}\left(\frac{\partial v}{\partial r} - \frac{v}{r} + \frac{1}{r}\frac{\partial u}{\partial\theta}\right) \tag{23}$$

where λ is Lamé's first parameter and $G_{r\theta}$ is the lateral soil shear modulus.

As presented in Fig. 1, a loading of $u = U_0e^{i\omega t}$ is applied in the direction of $\theta = 0^\circ$.

Potential functions φ and ψ, related to lateral u and tangential v displacements (Lamb, 1904), are expressed as

$$u = \frac{\partial\varphi}{\partial r} + \frac{1}{r}\frac{\partial\psi}{\partial\theta} \tag{24}$$

$$v = \frac{1}{r}\frac{\partial\varphi}{\partial\theta} - \frac{\partial\psi}{\partial r} \tag{25}$$

As for the axial analysis, two separate homogenous fields will be considered to model the nonlinear lateral pile vibrations.

4.2. Inner zone

The nonlinear inner zone solution is similar to that of a hollow cylinder (Lamb, 1904).

$$\phi = \left[C_1K_1\left(\frac{\alpha}{r_0}r\right) + C_2I_1\left(\frac{\alpha}{r_0}r\right)\right]cos\theta \tag{26}$$

$$\psi = \left[C_3K_1\left(\frac{\beta}{r_0}r\right) + C_4I_1\left(\frac{\beta}{r_0}r\right)\right]sin\theta \tag{27}$$

where C_1,C_2,C_3 and C_4 are constants depending on the boundary conditions, $\alpha = (\beta/\kappa)$ with $\kappa = \sqrt{(2(1-\upsilon)/(1-2\upsilon))}$, υ is the soil Poisson ratio, $\beta = (a_l i/\sqrt{1+i2\xi_{lat}})$, $a_l = (\omega r_0/V_{s,l})$ is the lateral dimensionless frequency, where ξ_{lat} is the hysteretic lateral damping, and $V_{s,l} = \sqrt{(G_{r\theta}/\rho)}$ is the shear wave velocity of the inner zone.

4.3. Outer zone

The solution for the outer zone is the same as that in Novak et al. (1978) for a semi-infinite medium (nonreflecting waves at $r=\infty$ or Sommerfeld radiation boundary condition), namely,

$$\phi = C_5K_1\left(\frac{\alpha_{max}}{r_0}r\right)cos\,\theta \tag{28}$$

$$\psi = C_6K_1\left(\frac{\beta_{max}}{r_0}r\right)sin\,\theta \tag{29}$$

where C_5 and C_6 are constants depending on the boundary conditions, $\alpha_{max} = (\beta_{max}/\kappa)$ where $\kappa = \sqrt{(2(1-\upsilon)/(1-2\upsilon))}$, υ is Poisson's ratio, $\beta = ((a_{l,max}i)/(\sqrt{1+i2\xi_{lat,min}}))$, where $\xi_{lat,min}$ is the equivalent hysteretic lateral damping in the outer zone, and $a_{l,max} = (\omega r_0/V_{s,l,max})$ is the dimensionless frequency, where $V_{s,l,max} = \sqrt{(G_{r\theta,max}/\rho)}$ is the shear wave velocity of the outer zone, with $G_{r\theta,max}$ being the lateral shear modulus in the outer zone.

4.4. Equivalent properties

Similar to the axial analysis (see Section 3.4), an equivalent linearization technique is used this time to calculate the degraded shear modulus and the hysteretic damping in the inner zone by iterations using an average lateral strain $\overline{\gamma}_{r\theta}$ in stress–strain constitutive Eq. (1) to (4.a–d). The expression for $\overline{\gamma}_{r\theta}$ is (Chau and Yang, 2005)

$$\overline{\gamma}_{r\theta} = \frac{1}{\pi(R_1^2 - r_0^2)}\int_0^{2\pi}\int_{r_0}^{R_1}|\gamma_{r\theta}rdrd\theta| \tag{30}$$

The iterations are stopped when the convergence of $\overline{\gamma}_{r\theta}$, $G_{r\theta}$ and ξ_{lat} has been reached.

4.5. Matrix formulation

Constants C_i, $i=1,6$ are determined by considering the following conditions:

1. Enforced displacement $U_0e^{i\omega t}$ at all points of the pile–soil interface.
2. Continuity of radial displacement u and tangential displacement v at the inner outer-zone interface.
3. Continuity of both radial stress σ_r and shear stress $\tau_{r\theta}$ across the two regions.

These conditions lead to six simultaneous equations which can be written in matrix form as

$$[L_{ij}]_{6\times6}C_i = U \tag{31}$$

where

$$C = \begin{bmatrix} C_1 & C_2 & C_3 & C_4 & C_5 & C_6 \end{bmatrix}^T \tag{32}$$

$$U = \begin{bmatrix} U_0 & -U_0 & 0 & 0 & 0 & 0 \end{bmatrix}^T \tag{33}$$

U_0 is the amplitude of the applied harmonic lateral displacement of all points of the pile–soil interface. It should be noted that the considered segment of the pile shaft itself undergoes a pure translation and remains circular.

The matrix elements, $[L_{ij}]_{6\times6}$, are expressed in Appendix B.

5. Numerical results of independent axial and lateral nonlinear soil responses

In this section, the numerical results that provide the nonlinear axial and lateral soil resistance to the imposed harmonic movement of the pile will be presented. The same dimensionless frequency, $a_0 = a_{max} = a_{l,max} = (\omega r_0/V_{s,max})$, is considered in either axial or lateral vibrations, allowing for $G_{rz,max} = G_{r\theta,max}$.

Table 1 summarizes the main reference parameters throughout this paper.

After the algorithm convergence of the axial analysis (Section 3.4), shear stress τ_{rz} at the pile–soil interface is expressed from Eq. (10). The complex axial dynamic impedance of the pile–soil system, per unit length of pile $K_{ax,nl}$, is obtained by

$$K_{ax,nl} = \frac{-2\pi r_0}{w_0}\tau_{rz}|_{r=r_0} \tag{34}$$

Eq. (34) is rewritten as

$$K_{ax,nl} = k_z + i\omega c_z \tag{35}$$

where k_z and ωc_z are the real and the imaginary parts of the axial soil–pile impedance of the pile shaft, respectively.

The reference linear impedance for the axial analysis (Novak et al., 1978) is expressed as

$$K_{ax,l} = 2\pi G_{rz,max}(1+i2\xi_{ax,min})\lambda_{max}\frac{H_1^2(\lambda_{max})}{H_0^2(\lambda_{max})} = k_{z,l} + i\omega c_{z,l} \tag{36}$$

H_0^2 and H_1^2 are the second kind Henkel function of the zero and the first order, respectively.

For the sake of comparison, the stiffness and the dashpot coefficients ($k_{gaztas,nl}$ and $c_{gaztas,nl}$) of the model by Michaelides et al. (1997, 1998) are used in this section to analyze the axial soil impedance. Michaelides et al. (1997, 1998) used a radial discretization of the soil with parabolic distribution of the shear modulus based on the experimental law of Ishibashi and Zhang (1993). The approximate form of the solution by Michaelides et al. (1997, 1998) results in

$$k_{gaztas,nl} = (1+1.2\lambda)^{-1}\left(1-\frac{0.6\lambda}{1-\lambda}a^{1.5}\right)k_{gaztas,l} \tag{37}$$

$$c_{gazetas,nl} = (1-0.84\lambda(1+0.66log\ a))c_{gazetas,l} \tag{38}$$

where λ is the loading intensity parameter, $\lambda = 600(\tau_{rz,max}/G_{rz,max})e^{-1.39(PI/125)}$, while $k_{gazetas,l} = 1.8G_{rz,max}(1+0.5\sqrt{a_{max}})$ and $c_{gazetas,l} = 2.4a_{max}^{0.25}\pi r_0\rho V_{s,max} + 2\xi_{rz,min}(k_{gazetas,l}/\omega)$ are the real and the imaginary linear (λ=0) impedance parameters, respectively, according to Makris and Gazetas (1993).

After the convergence of the iterative procedure discussed in Section 4.4, the complex lateral soil impedance is derived from horizontal soil resistance P. The latter is calculated based on the following expression:

$$P(r) = -\int_0^{2\pi}(\sigma_r(r,\theta)cos(\theta) - \tau_{r\theta}(r,\theta)sin(\theta))rd\theta \tag{39}$$

The nonlinear lateral soil impedance is expressed as

$$K_{lat,nl} = \frac{P|_{r=r_0}}{U_0} \tag{40}$$

Eq. (40) is rewritten as

$$K_{lat,nl} = k_h + i\omega c_h \tag{41}$$

where k_h and ωc_h are the real and the imaginary parts of the lateral soil–pile impedance of the pile shaft.

k_z, c_z, k_h and c_h are frequency-dependent (they also incorporate hysteric damping); they represent lateral spring and dashpot constants of the pile–soil interface model.

Table 1
Summary of reference parameters used in numerical analysis.

ρ[kg/m^3]	IP	$\gamma_{ref}(\sigma_r')$	c[kPa]	δ [°]	e	ν	σ'[kPa]	r_0[m]	$\xi_{ax,min}$	$\xi_{lat,min}$
1800	50	3×10^{-4}	0	30°	0.8	0.4	30	0.2	0.01	0.01

For the lateral analysis, Novak et al. (1978)'s linear impedance is expressed as

$$K_{h,l} = -\pi a_{max}^2 G_{r\theta,max} T = k_{h,l} + i\omega c_{h,l} \tag{42}$$

where

$$T = \frac{4H_1^2(\beta_{max})H_1^2(\alpha_{max}) + \alpha_{max}H_1^2(\beta_{max})H_0^2(\alpha_{max}) + \beta_{max}H_0^2(\beta_{max})H_1^2(\alpha_{max})}{\beta_{max}H_0^2(\beta_{max})H_1^2(\alpha_{max}) + \alpha_{max}H_1^2(\beta_{max})H_0^2(\alpha_{max}) + \beta_{max}\alpha_{max}H_0^2(\beta_{max})H_0^2(\alpha_{max})} \tag{43}$$

Figs. 3 and 4 represent the real and the imaginary parts, respectively, of the axial soil–pile impedance derived from the approach presented in Section 3 under imposed vertical pile displacement $W_0 = 0.001r_0$. Likewise, Figs. 5 and 6 represent the real and the imaginary parts, respectively, of the lateral soil–pile impedance derived from the approach presented in Section 4 under imposed lateral pile displacement $U_0 = 0.0001r_0$.

These impedances are normalized to the axial ($k_{z,l}$,$c_{z,l}$) and to the lateral ($k_{h,l}$ $c_{h,l}$) linear impedances derived by Novak et al. (1978), assuming $\xi_{ax,min} = \xi_{lat,min} = 0.01$, to better visualize their nonlinear character. Figs. 3–6 provide the results for different dimensionless inner zone radii; R_1/r_0 values 1.5, 2, 3 and 6 are considered.

The value of R_1/r_0 to be adopted for particular cases has been debated in literature. It can be expected to depend on the extent of the nonlinearity, and thus, to the level of loading. Chau and Yang (2005) used a ratio of R_1/r_0 varying from 1.5 to 5 for the parametric analysis. Han and Sabin (1995) used a ratio of R_1/r_0 varying from 1.1 to 2. The selection of the R_1/r_0 ratio could be based on experimental observation (dynamic t-z or P-y matching). NCHRP report 461 (2001) suggests using R_1/r_0 values ranging from 1.1 to 2.

Both stress–strain relations presented in Section 2 are used in the analysis. The results are presented for the frequency range of $0.01 < a_0 < 1$, which is the range of practical interest (Makris and Gazetas 1993).

It was found from Figs. 3–6 that

1. The evaluated solutions conform to the expectation that the nonlinear soil reaction does not exceed that evaluated by Novak et al. (1978)'s, which assumes viscoelastic behavior. This is unlike the solution by Michaelides et al. (1997, 1998) for the axial case, where the values of $k_{gaztas,nl}$ and $c_{gaztas,nl}$ can unplausibly exceed their viscoelastic counterparts.

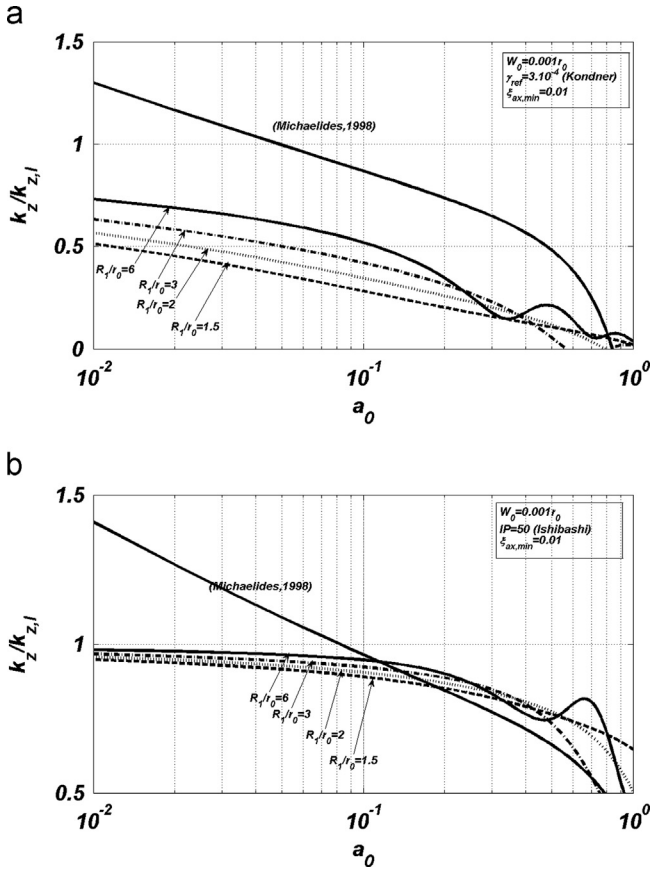

Fig. 3. Nonlinear axial soil stiffness for four inner zone radii using the stress–strain law of (a) Kondner ($\gamma_{ref} = 3 \times 10^{-4}$) and (b) Ishibashi (IP = 50), under $W_0 = 0.001r_0$.

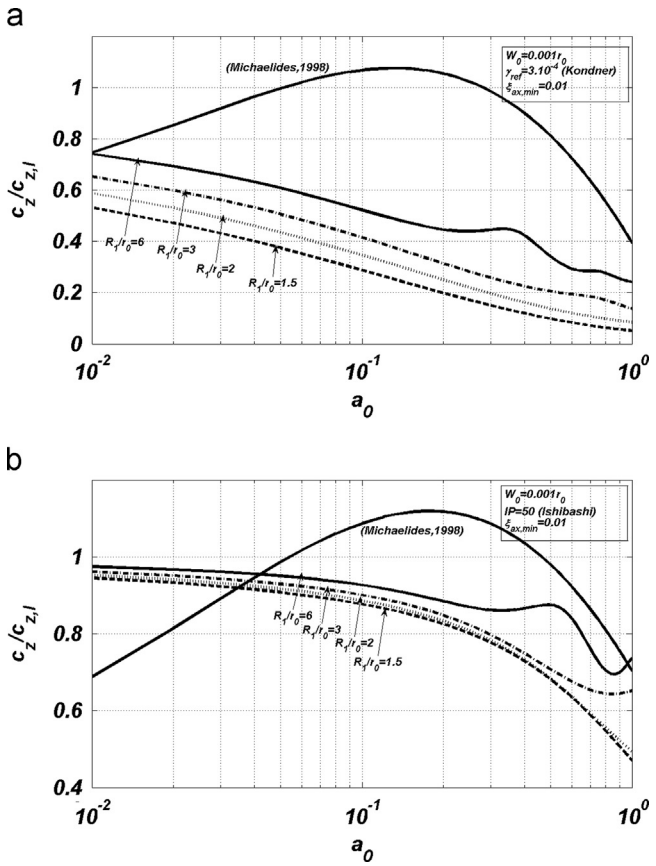

Fig. 4. Nonlinear axial soil damping for four inner zone radii using the stress–strain law of (a) Kondner ($\gamma_{ref} = 3 \times 10^{-4}$) and (b) Ishibashi (IP = 50), under $W_0 = 0.001r_0$.

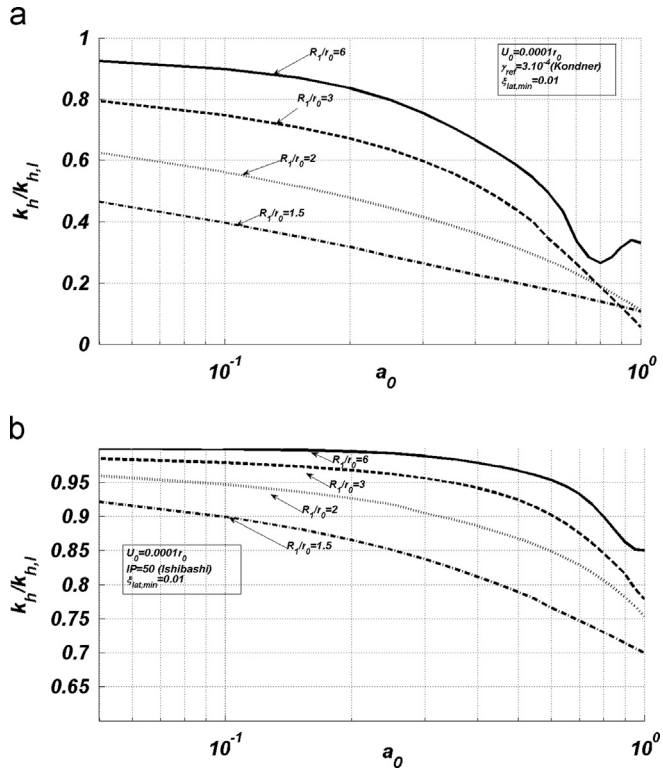

Fig. 5. Nonlinear lateral soil stiffness for four inner zone radii using the stress–strain law of (a) Kondner ($\gamma_{ref}=3\times10^{-4}$) and (b) Ishibashi (IP=50), under $U_0=0.0001r_0$.

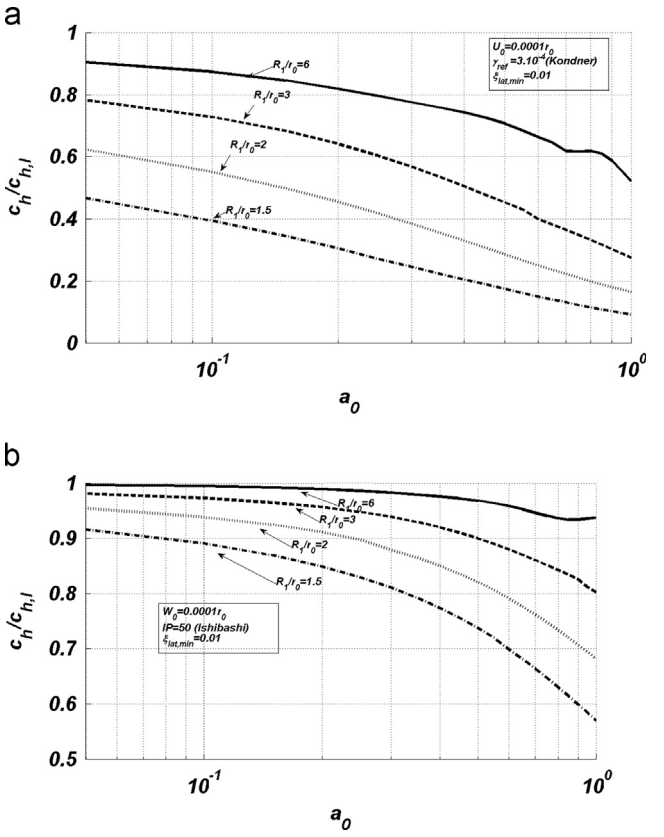

Fig. 6. Nonlinear lateral soil damping for four inner zone radii using the stress–strain law of (a) Kondner ($\gamma_{ref}=3\times10^{-4}$) and (b) Ishibashi (IP=50), under $U_0=0.0001r_0$.

2. The radius of the inner zone is of great importance in the analysis, since nonlinear stiffness and dashpot constants increase with R_1/r_0 values. This is an expected result, since higher degradation is observed for lower inner zone radii, reflecting the geometric attenuation of the deformation amplitude with the radial coordinate. In the authors' opinion, the strongly degraded inner zone (in practical situations involving vibratory pile driving, impact pile driving and so on) should not extend twice the radius of the pile.
3. The degradation of the soil stiffness and dashpot constants increases when dimensionless frequency a_0 increases.
4. Kondner's law with $\gamma_{ref}=3\times10^{-4}$ results in a more extensive stiffness degradation than Ishibashi and Zhang's law with IP=50, which is in accordance with the observations made in Fig. 2a.

The authors noted that, in the course of the iterative procedure discussed in Sections 3.4 and 4.4, convergence could generally be reached in less than 20 steps for both axial and lateral analyses, which is required to establish Figs. 3–6. It was also noticed that a larger number of steps would occasionally be needed to assure convergence for higher frequencies and higher imposed displacements.

For both axial and lateral analyses, strain levels ($\overline{\gamma}_{rz}$, $\overline{\gamma}_{r\theta}$) vary from $\gamma_{ref}/2$ for lower displacement ($W_0=10^{-4}r_0$ and $U_0=10^{-5}r_0$) and lower dimensionless frequency ($a_{max}=0.1$) to $4\gamma_{ref}$ for higher displacement ($W_0=10^{-3}r_0$ and $U_0=10^{-4}r_0$) and higher dimensionless frequency ($a_{max}=0.5$).

Figs. 7 and 8 show that with an inner radius of $R_1/r_0=1.5$ with Kondner's law, a progressive decrease in the amplitude of the imposed displacements induces a progressive increase in soil stiffness. For vanishing displacements (axial W_0 less than $10^{-5}r_0$ and lateral U_0 less than $10^{-6}r_0$), the proposed solutions coincide with the viscoelastic solution developed by Novak et al. (1978). The same conclusions were drawn by the authors for axial and lateral damping. This validates the proposed nonlinear algorithms for axial and lateral analyses with reference to the equivalent linear case.

6. Numerical results for coupling analysis

When both lateral and axial in-phase harmonic displacements simultaneously occur $\left(\left\{\underset{x}{U_0},0_y,\underset{z}{W_0}\right\}e^{i\omega t}\right)$, the axial ultimate resistance of the pile shaft is influenced by variations in the radial soil stress (Horikoshi et al., 2003; Matsumoto et al., 2004; Nishimura et al., 2012). This is easily expressed using the Mohr–Coulomb criterion for cohesionless soil.

$$\tau_{rz,max}=\sigma_r'\tan\delta \tag{44}$$

Consequently, the calculation of the updated radial stress value at the pile–soil interface, due to the lateral displacement, is very important for seeing whether or not there is a change in maximum axial shear $\tau_{rz,max}$. In Fig. 9, the evolution of the radial stress amplitude around the pile, for a given

dimensionless frequency $a_0=0.1$, is investigated. Beginning with the initial radial stress calculated from the coefficient of lateral stress at rest, k (green circle in Fig. 9, the blue circles represent the evolution of the radial stress for different values of imposed displacement U_0/r_0. The radial stress distribution results from the nonlinear algorithms presented in Section 4 for the lateral soil vibrations after reaching convergence. It is noted that the radial stress on the left side decreases until the active limit state is reached (red circle). The active limit constitutes a lower bound for the radial stress in this case. On the right side; however, the inverse situation happens. The radial stress increases and approaches the passive limit state (red circle). This state constitutes a higher bound, since the radial stress should not exceed the passive radial stress.

An elliptical shape of the radial stress distribution is obtained before reaching the active limit state. Reaching the passive limit state requires rather large lateral displacements (more than $r_0/10$ in this case).

Attention must be paid to the circumferential distributions of radial and tangential displacements within the soil. Results show that the radial displacement and stress are maximum at the angle of imposed loading ($\theta=0^\circ$), while the maximum values for the tangential displacement and shear strain (and shear stress) are maximum at angle $\theta=90^\circ$. This emphasizes the fact that the average shear strain, chosen per Eqs. (15) and (30), remains an approximation. These circumferential distributions have to be taken into account when analyzing the coupling between axial and lateral responses. In fact, it is necessary to compute an average value for the radial stress for the calculation of the coupled maximum shear stress (Eq. (44)).

This was calculated using the following equation:

$$\sigma_{r,\mathrm{avg}}{}' = \frac{1}{2\pi}\int_0^{2\pi} \sigma'_{r|r=r_0} d\theta \tag{45}$$

The evolution of the radial average stress at the soil–pile interface is presented in Fig. 10 for the stress–strain relationships presented in Section 2, for two values of the dimensionless frequency ($a_0=0.1$ and $a_0=0.5$) and for three values of R_1/r_0(1.5, 2 and 3).

It was found from Fig. 10 that

1. $\sigma_{r,\mathrm{avg}}{}'$ remains constant under limited lateral displacements. This value is equal to initial radial stress $\sigma'_{r,0}$.
2. Beyond a certain imposed displacement U_0 (threshold displacement), which corresponds to the beginning of the plastic state (soil active state in Fig. 9), the radial mean stress increases quasi-linearly.

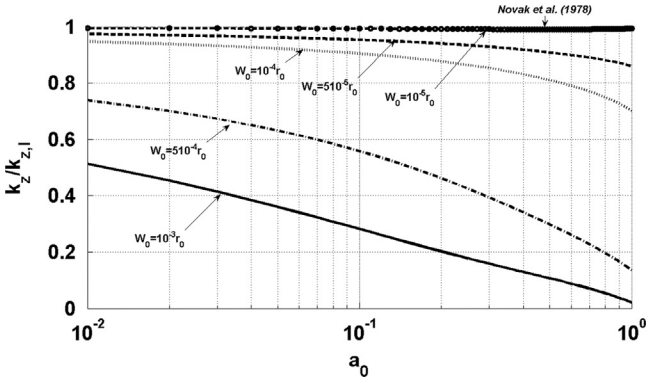

Fig. 7. Axial stiffness validation for $R_1/r_0=1.5$ with Kondner law.

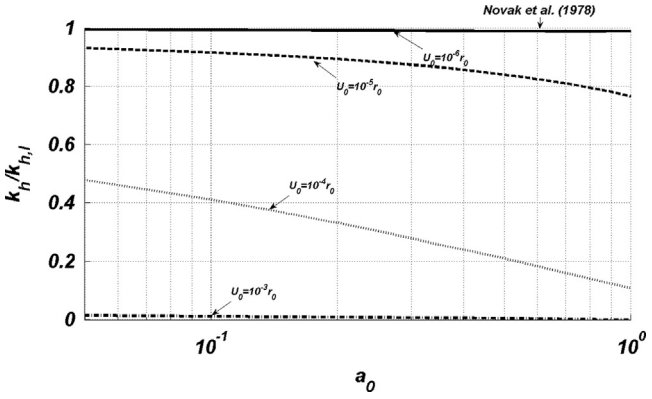

Fig. 8. Lateral stiffness validation for $R_1/r_0=1.5$ with Kondner law.

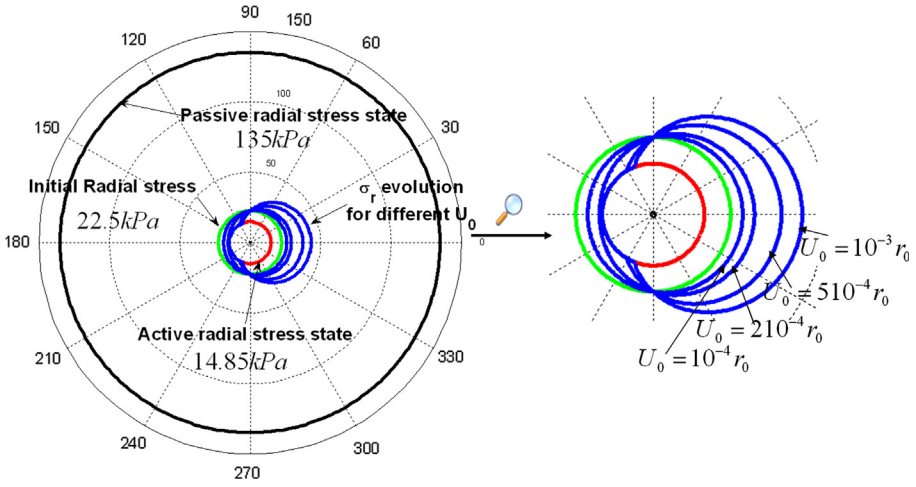

Fig. 9. Evolution of peak radial stress amplitude as function of lateral pile displacement using Kondner for $a_0=0.1$. (For interpretation of the references to color in this figure legend, the reader is referred to the web version of this article.)

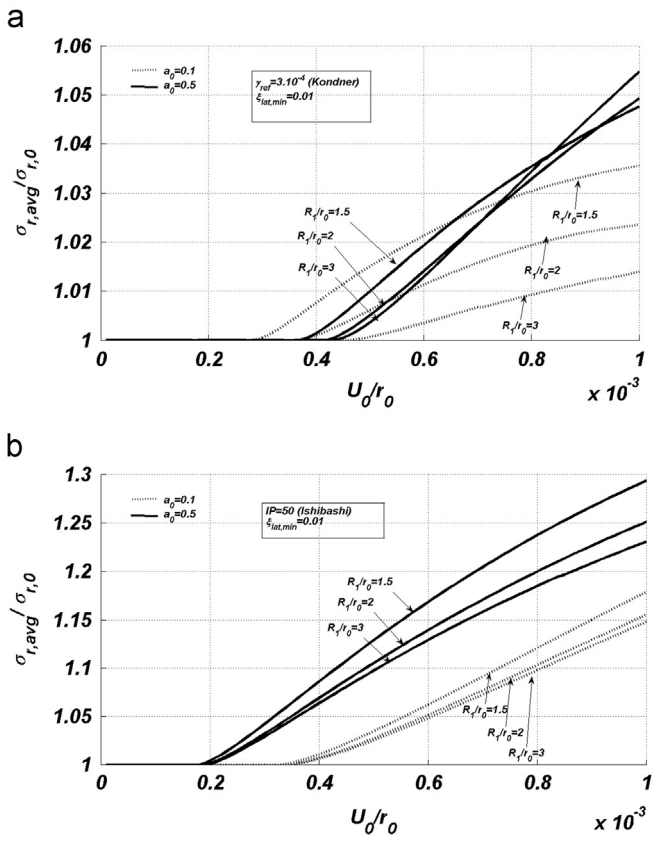

Fig. 10. Mean radial stress versus lateral pile displacement using law of (a) Kondner ($\gamma_{ref}=3\times10^{-4}$) and (b) Ishibashi (IP=50), for two dimensionless frequencies ($a_0=0.1$ and $a_0=0.5$) and three inner zone radii.

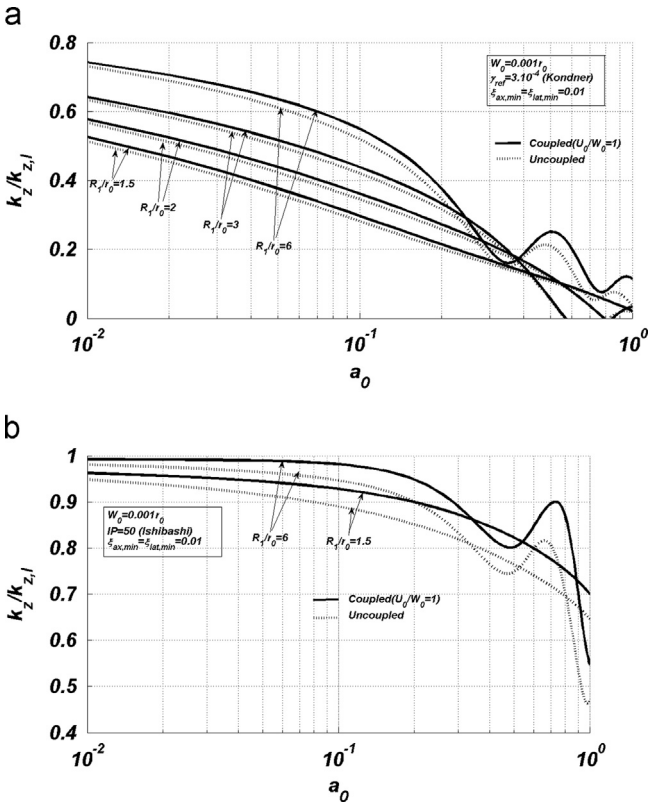

Fig. 11. Coupled and uncoupled axial soil stiffness using law of (a) Kondner ($\gamma_{ref}=3\times10^{-4}$) and (b) Ishibashi (IP=50) under $W_0=0.001r_0$ for two inner zone radii.

3. Since the lateral soil stiffness decreases with the dimensionless frequency, the soil enters into the state of plasticity more rapidly.
4. $\sigma_{r,avg}{}'$ increases more rapidly for low values of R_1/r_0.

A second coupling effect between axial and lateral loading applies to the maximum soil shear modulus. In fact, according to Eq. (6), G_{max} depends on the confining stress which, in turn, depends on the nonlinear mean radial stress. Consequently, a change in the radial stress also implies a change in G_{max}, according to Eqs. (4) and (5). When using Ishibashi and Zhang's approach, the stress–strain relation also depends on the confining stress, thus, causing another coupling between the axial and lateral vibrations.

Figs. 11 and 12 compare the coupled nonlinear axial soil stiffness and damping constants to the uncoupled ones for imposed vertical displacement amplitude $W_0=10^{-3}r_0$. It can be noted that

1. The increase in the coupled soil axial stiffness and dashpot constants, relative to the uncoupled ones, is more pronounced for a ratio of $U_0/W_0=1$.
2. The gain in axial soil reaction is not very significant for the imposed displacements (in the order of 2–3% of the linear soil stiffness and dashpot constants and 10% of the nonlinear soil stiffness and dashpot constants).
3. For a given value of R_1/r_0, the gain in axial soil resistance seems to be constant.

Figs. 13 and 14 portray the coupling effect for a higher imposed displacement ($W_0=10^{-2}r_0$ being in the range of practical interest of pile driving and vibratory pile driving). It was concluded from Figs. 13 and 14 such that

1. The coupling effects begin for a displacement ratio of $U_0/W_0=0.1$. For a U_0/W_0 value lower than 0.1, no coupling was observed as the coupled soil impedance coincides with the uncoupled nonlinear axial soil impedance.
2. The coupled nonlinear soil stiffness and damping increase for higher values of U_0/W_0. This is in accordance with the results of Fig. 10.
3. For a U_0/W_0 value of 1, the coupled axial soil reaction increases by about 50% compared to the uncoupled one.
4. Higher R_1/r_0 ratios induce higher coupling effects for the same value of U_0/W_0.

Figs. 15 and 16 illustrate the respective influences of hysteretic damping ξ_{min} ($\xi_{min}=\xi_{ax,min}=\xi_{lat,min}$) and of Poisson's

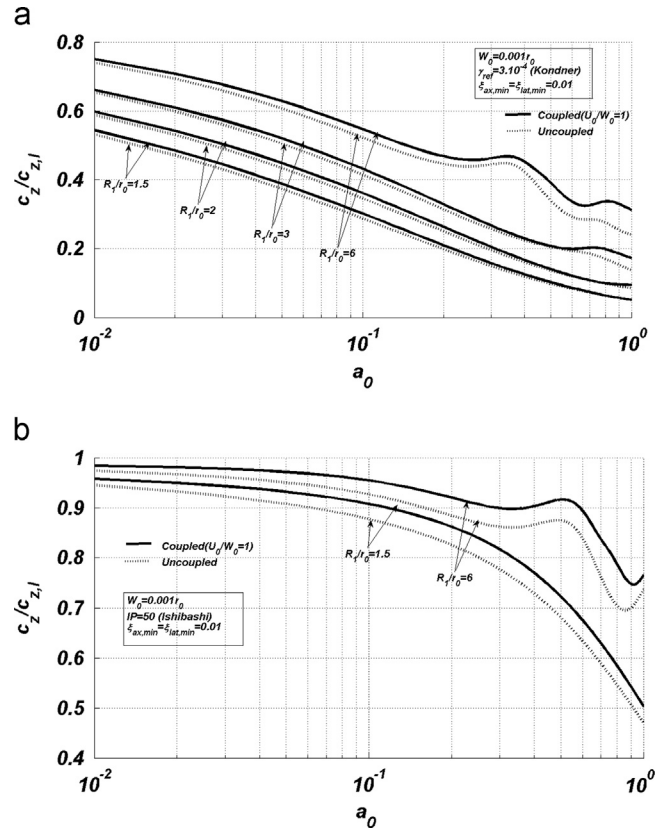

Fig. 12. Coupled and uncoupled axial soil damping using law of (a) Kondner ($\gamma_{ref}=3\times10^{-4}$) and (b) Ishibashi (IP=50) under $W_0=0.001r_0$ for two inner zone radii.

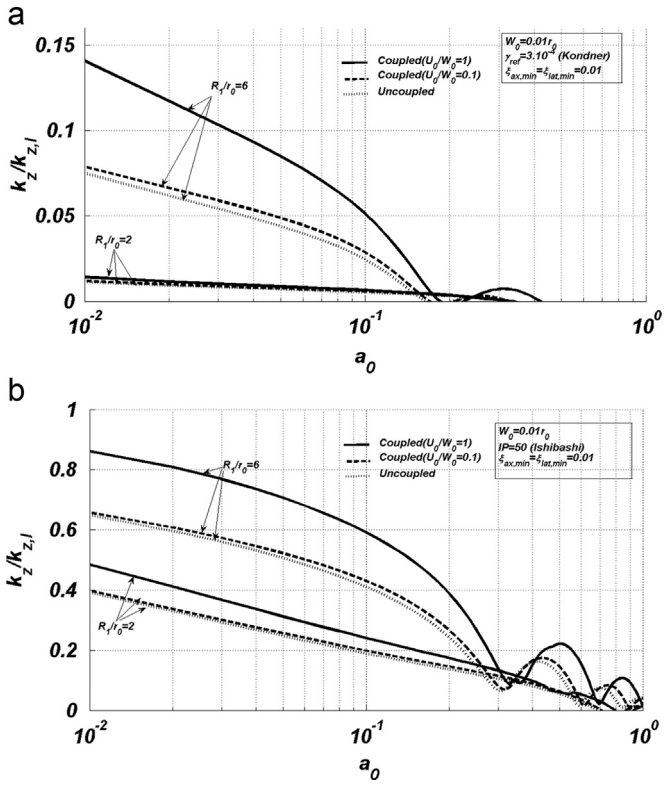

Fig. 13. Coupled and uncoupled axial soil stiffness using law of (a) Kondner ($\gamma_{ref}=3\times10^{-4}$) and (b) Ishibashi (IP=50) under $W_0=0.01r_0$ for two inner zone radii.

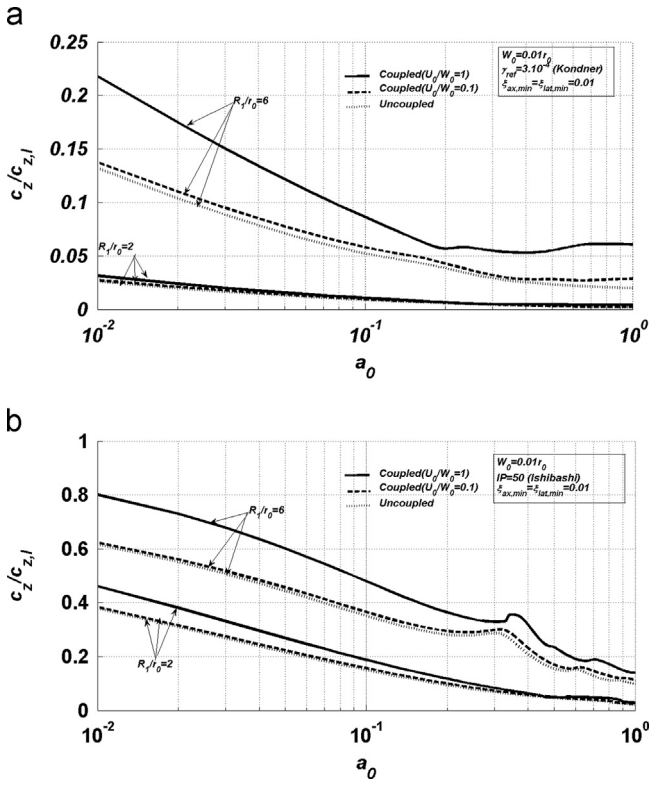

Fig. 14. Coupled and uncoupled axial soil damping using law of (a) Kondner ($\gamma_{ref}=3\times10^{-4}$) and (b) Ishibashi (IP=50) under $W_0=0.01r_0$ for two inner zone radii.

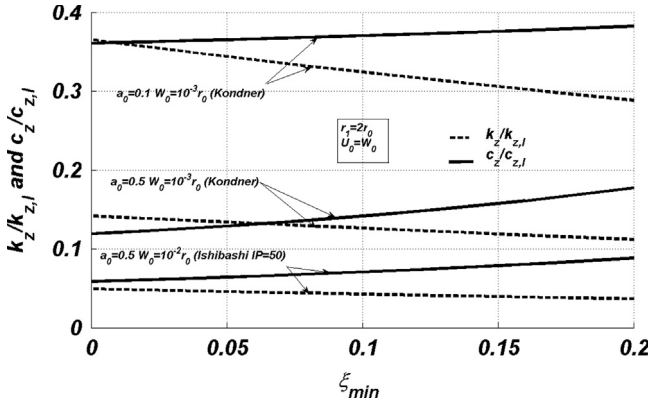

Fig. 15. Influence of the outer zone hysteretic damping on coupled nonlinear axial impedance for $r_1=2r_0$ and $U_0=W_0$.

ratio on the coupled soil impedance for two different dimensionless frequencies (a_0=0.1 and a_0=0.5), combined with selected displacement and degradation laws.

It can be observed from Fig. 15 that the coupled normalized stiffness decreases when the hysteretic damping of the outer zone increases, while the opposite happens for the coupled normalized damping. This is in agreement with the equivalent viscoelastic analysis of Novak et al. (1978). The same conclusions were found for uncoupled normalized stiffness and damping.

The logarithmic scale used in Fig. 16 helps the reader detect the modest increase in the coupled impedance for a higher

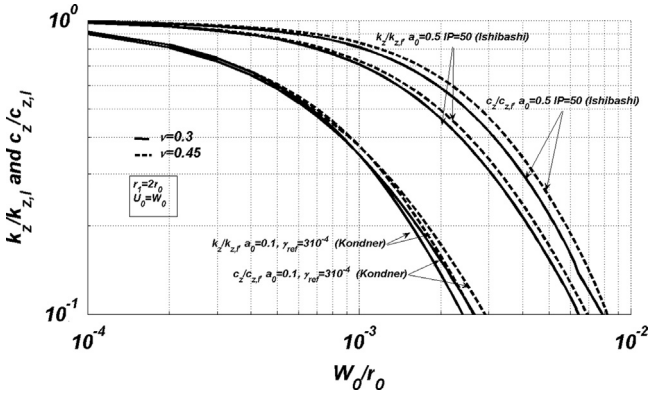

Fig. 16. Coupled nonlinear axial impedance of shaft pile vs. dimensionless displacement for $\nu=0.3$ and $\nu=0.45$ ($r_1=2r_0$ and $U_0=W_0$).

Poisson's ratio, provided that the dimensionless displacement exceeds $W_0=10^{-3}r_0$.

7. Conclusions

In this paper, a nonlinear axial and lateral soil analysis, based on an extension of the available plane strain solution, is developed for the purpose of coupling the axial and lateral in-phase pile harmonic responses of a pile shaft. A plane strain soil disk was assumed, using an inner nonlinear zone and an outer visco-elastic zone, for both axial and lateral vibrations. It was shown that the radial mean stress increases significantly as a function of the lateral soil displacement, resulting in an increase in the axial soil stiffness and damping when using Kondner's hyperbolic law. That increase in the radial mean stress also induces an increase in the mean effective stress which, in turn, induces an increase in the soil stiffness when using Ishibashi and Zhang's law. The developed solutions are useful for managing nonaxial soil loading (vibratory pile driving, offshore piles, windmill pile foundations and so on) and for estimating the effects on axial pile vibrations. A practical conclusion is that the axial resistance of piles undergoing lateral displacement can be increased from a purely axial one by a margin in the order of 10% for limited lateral displacements and much more (up to 50%) under more intense lateral displacements.

Appendix A

$$A_{11}=K_0(\lambda) \qquad A_{12}=I_0(\lambda) \qquad A_{13}=0$$

$$A_{21}=K_0\left(\frac{\lambda}{r_0}R_1\right) \qquad A_{22}=I_0\left(\frac{\lambda}{r_0}R_1\right) \qquad A_{23}=-K_0(\lambda_{max})$$

$$A_{31}=-\frac{\lambda}{r_0}K_1\left(\frac{\lambda}{r_0}R_1\right) A_{32}=\frac{\lambda}{r_0}I_1\left(\frac{\lambda}{r_0}R_1\right)$$

$$A_{33}=\frac{G_{rz,max}(1+i2\xi_{ax,min})}{G_{rz}(1+i2\xi_{ax})}\frac{\lambda_{max}}{R_1}K_1(\lambda_{max})$$

Appendix B

It should be noted that the expressions below, although inspired from the methodology proposed by Chau and Yang (2005), are different. Chau and Yang (2005) extended Novak and Nogami (1977)'s solution; however, the expressions below are an extension of Novak et al. (1978)'s solution under plane strain conditions.

$$L_{11}=\frac{1}{r_0}K_1(\alpha)+\frac{\alpha}{r_0}K_0(\alpha) \qquad L_{12}=\frac{1}{r_0}I_1(\alpha)-\frac{\alpha}{r_0}I_0(\alpha)$$

$$L_{13}=-\frac{1}{r_0}K_1(\beta) \qquad L_{14}=-\frac{1}{r_0}I_1(\beta)$$

$$L_{15}=0 \qquad L_{16}=0$$

$$L_{21}=\frac{1}{r_0}K_1(\alpha) \qquad L_{22}=\frac{1}{r_0}I_1(\alpha)$$

$$L_{23}=-\left(\frac{1}{r_0}K_1(\alpha)+\frac{\alpha}{r_0}K_0(\alpha)\right) \qquad L_{24}=-\left(\frac{1}{r_0}I_1(\alpha)+\frac{\alpha}{r_0}I_0(\alpha)\right)$$

$$L_{25}=0 \qquad L_{26}=0$$

$$L_{31}=\frac{1}{R_1}K_1\left(\frac{\alpha}{r_0}R_1\right)+\frac{\alpha}{r_0}K_0\left(\frac{\alpha}{r_0}R_1\right) \qquad L_{32}=\frac{1}{R_1}I_1\left(\frac{\alpha}{r_0}R_1\right)-\frac{\alpha}{r_0}I_0\left(\frac{\alpha}{r_0}R_1\right)$$

$$L_{33}=\frac{1}{R_1}K_1\left(\frac{\alpha}{r_0}R_1\right) \qquad L_{34}=-\frac{1}{R_1}I_1\left(\frac{\alpha}{r_0}R_1\right)$$

$$L_{35}=\frac{1}{R_1}K_1(\alpha_{max})+\frac{\alpha_{max}}{R_1}K_0(\alpha_{max}) \qquad L_{36}=\frac{1}{R_1}K_1(\beta_{max})$$

$$L_{41}=\frac{1}{R_1}K_1\left(\frac{\alpha}{r_0}R_1\right) \qquad L_{42}=\frac{1}{R_1}I_1\left(\frac{\alpha}{r_0}R_1\right)$$

$$L_{43}=-\left(\frac{1}{R_1}K_1\left(\frac{\alpha}{r_0}R_1\right)+\frac{\alpha}{r_0}K_0\left(\frac{\alpha}{r_0}R_1\right)\right) \qquad L_{44}=-\left(\frac{1}{R_1}I_1\left(\frac{\alpha}{r_0}R_1\right)-\frac{\alpha}{r_0}I_0\left(\frac{\alpha}{r_0}R_1\right)\right)$$

$$L_{45}=-\frac{1}{R_1}K_1(\alpha_{max}) \qquad L_{46}=\frac{1}{R_1}K_1(\beta_{max})+\frac{\beta_{max}}{R_1}K_0(\beta_{max})$$

$$L_{51}=\left(\kappa\frac{\alpha}{r_0}\right)^2K_1\left(\frac{\alpha}{r_0}R_1\right)+\frac{4}{R_1^2}K_1\left(\frac{\alpha}{r_0}R_1\right)+\frac{2\alpha}{r_0R_1}K_0\left(\frac{\alpha}{r_0}R_1\right)$$

$$L_{52}=\left(\kappa\frac{\alpha}{r_0}\right)^2I_1\left(\frac{\alpha}{r_0}R_1\right)+\frac{4}{R_1^2}I_1\left(\frac{\alpha}{r_0}R_1\right)-\frac{2\alpha}{r_0R_1}I_0\left(\frac{\alpha}{r_0}R_1\right)$$

$$L_{53}=-\left(\frac{4}{R_1^2}K_1\left(\frac{\beta}{r_0}R_1\right)+\frac{2\beta}{r_0R_1}K_0\left(\frac{\beta}{r_0}R_1\right)\right)$$

$$L_{54}=-\left(\frac{4}{R_1^2}I_1\left(\frac{\beta}{r_0}R_1\right)-\frac{2\beta}{r_0R_1}I_0\left(\frac{\beta}{r_0}R_1\right)\right)$$

$$L_{55}=\left(-\frac{G_{r\theta,max}(1+i2\xi_{lat,min})}{G_{r\theta}(1+i2\xi_{lat})}\right)\times\left[\left(\frac{\kappa\alpha_{max}}{R_1}\right)^2K_1(\alpha_{max})+\frac{4}{R_1^2}K_1(\alpha_{max})+\frac{2\alpha_{max}}{R_1^2}K_0(\alpha_{max})\right]$$

$$L_{56}=\left(-\frac{G_{r\theta,max}(1+i2\xi_{lat,min})}{G_{r\theta}(1+i2\xi_{lat})}\right)\left[\frac{4}{R_1^2}K_1(\beta_{max})+\frac{2\alpha_{max}}{R_1^2}K_0(\beta_{max})\right]$$

$$L_{61}=\frac{4}{R_1^2}K_1\left(\frac{\alpha}{r_0}R_1\right)+\frac{2\alpha}{r_0R_1}K_0\left(\frac{\alpha}{r_0}R_1\right)$$

$$L_{62}=\frac{4}{R_1^2}I_1\left(\frac{\alpha}{r_0}R_1\right)-\frac{2\alpha}{r_0R_1}I_0\left(\frac{\alpha}{r_0}R_1\right)$$

$$L_{63}=-\left(\frac{\beta}{r_0}\right)^2K_1\left(\frac{\beta}{r_0}R_1\right)+\frac{4}{R_1^2}K_1\left(\frac{\beta}{r_0}R_1\right)+\frac{2\beta}{r_0R_1}K_0\left(\frac{\beta}{r_0}R_1\right)$$

$$L_{64} = -\left(\frac{\beta}{r_0}\right)^2 I_1\left(\frac{\beta}{r_0}R_1\right) + \frac{4}{R_1^2} I_1\left(\frac{\beta}{r_0}R_1\right) - \frac{2\beta}{r_0 R_1} I_0\left(\frac{\beta}{r_0}R_1\right)$$

$$L_{65} = \left(-\frac{G_{r\theta,max}(1+i2\xi_{lat,min})}{G_{r\theta}(1+i2\xi_{lat})}\right)\left[\frac{4}{R_1^2}K_1(\alpha_{max}) + \frac{2\alpha_{max}}{R_1^2}K_0(\alpha_{max})\right]$$

$$L_{66} = \left(\frac{G_{r\theta,max}(1+i2\xi_{lat,min})}{G_{r\theta}(1+i2\xi_{lat})}\right) \times \left[\left(\frac{\alpha_{max}}{R_1}\right)^2 K_1(\beta_{max}) + \frac{4}{R_1^2}K_1(\beta_{max}) + \frac{2\alpha_{max}}{R_1^2}K_0(\beta_{max})\right]$$

References

API, 1991. Recommended Practice for Planning, Designing and Constructing Fixed Offshore Platforms, 19th edition American Petroleum Institute, Dallas, Texas API Recommended Practice 2A.

Abramowitz, M., Stegum, I.A., 1972. Handbook of Mathematical Functions. Dover Publications, New York.

Bolton M.D.,1991. Geotechnical Stress Analysis: A Possible Approach for Cantilever Retaining Walls on Spread Foundations. TRRL, contractor Report 271, Berkshire :28.

Brumund, W.F., Leonerds, G.A., 1973. Experimental study of static and dynamic friction between sand and typical construction materials. Journal of Testing and Evaluation 2, 162–165.

Chau, K.T., Yang, X., 2005. Nonlinear interaction of soil-pile in horizontal vibration. Journal of Engineering Mechanics ACSE 131 (8), 847–858.

El Naggar, H., Novak, M., 1994a. Nonlinear axial interaction in pile dynamics. Journal of Geotechnical Engineering ASCE 120 (4), 678–696.

El Naggar H., Novak M. 1994b. Nonlinear model for dynamic axial pile response. Journal of Geotechnical Engineering ASCE 120 (2), 308–329.

El Naggar M.H., Novak M. 1995. Nonlinear lateral interaction in pile dynamics, Soil Dynamics and Earthquake Engineering 14, 141–157.

El Naggar M.H., Novak M. 1996. Nonlinear analysis for dynamic lateral pile response. Soil Dynamics and Earthquake Engineering 15 (4), 223–244.

Han Y.C., Sabin G.C.W. 1995. Impedances for radially inhomogeneous viscoelastic soil media. Journal of the Engineering Mechanics Division ASCE (110) 6, 939–947.

Hardin B.O. 1978. The nature of stress-strain behaviour for soils. Earthquake Engineering and Soil Dynamics ASCE (1) 3–89.

Hardin, B.O., Drnevich, V.P., 1972. Shear modulus and damping in soils. Measurement and parameter effects. Journal of the Soil Mechanics and Foundations Division 98 (6), 603–624.

Holeyman A.E., 1992. Keynote lecture: Technology of pile dynamics. Proceedings of the Fourth International Conference on the Application of Stress Wave Theory to Piles 195–215. A.A BALKEMA, Rotterdam, Netherlands.

Horikoshi, K., Matsumoto, T., Hashizume, Y., Watanabe, T., 2003. Performance of piled raft foundations subjected to dynamic loading. International Journal of Physical Modelling in Geotechnics 3 (2), 51–62.

Ishibashi I., Zhang X. 1993. Unified shear moduli and damping ratios of sand and clay. Soils and Foundations 33, 182–191.

Ishihara, K., 1996. Soil Behaviour in Earthquake Geotechnics. Oxford Clarendon Press.

Jardine R.J., Standing J.R. 2012. Field axial cyclic loading experiments on piles driven in sand. Soils and Foundations 52, 723–736.

Jardine, R.J., Lehane, B.M., Everton, S.J., 1992. Friction coefficients for piles in sands and silts. Proceedings of International Conference on Offshore Site Investigation and Foundation Behaviour. STU London, Kluwer (Dordrecht) 661–677.

Jardine, R.J., Chow, F., Overy, R., Standing, J., 2005. ICP Design Methods for Driven Piles in Sands and Clays. Thomas Telford Ltd 15–21.

Kondner R.L., 1963. Hyperbolic stress strain response: cohesive soils. Journal of Soil Mechanics and Foundations Division 189, 115–143.

Kramer, S., 1996. Geotechnical Earthquake Engineering, 1st edition Prentice Hall.

Lamb H. 1904. On the propagation of tremors over the surface of an elastic solids. Philosophical Transactions of the Royal Society London Series A. 203, 1–42.

Makris, N., Gazetas, G., 1993. Displacement phase differences in a harmonically oscillating pile. Geotechnique 43, 135–150.

Matsumoto, T., Fukumura, K., Kitiyodom, P., Oki, A., Horikoshi, K., 2004. Experimental and analytical study on behaviour of model piled rafts in sand subjected to horizontal and moment loading. International Journal of Physical Modelling in Geotechnics 4 (3), 1–19.

Michaelides O., Gazetas G. 1995. Discussion of 'impedance functions of piles in inhomogeneous media. Journal of Geotechnical Engineering 121 (2), 235–236.

Michaelides O., Gazetas G., Bouckovalas G., Chrysikou E. 1997. Approximate non-linear dynamic axial response of piles. Géotechnique 48 (4), 33–53.

Michaelides, O., Bouckovalas, G., Gazetas, G., 1998. Non-linear soil properties and impedances for axially vibrating elements. Journal of the Japanese Geotechnical Society: Soils and Foundations 38 (3), 129–142.

Mitwally H. Novak M. 1988. Pile driving analysis using shaft and FEM. Proceedings of the Third International Conference on the Application of Stress Wave Theory to Piles Bitech Publishers, Vancouver.

NCHRP report 461, 2001. Static and Dynamic Lateral Loading of Pile Groups. National Academy Press, Washington, D.CB15.

Nishimura S., Takahashi H., Morikawa Y. 2012. Observations of dynamic and non-dynamic interactions between a quay wall and partially stabilised backfill. Soils and Foundations 52 (1), 81–98.

Nogami, T., Novak, M., 1977. Resistance of soil to a horizontally vibrating pile. Earthquake Engineering and Structural Dynamics 249, 261–265.

Novak M. 1974. Dynamic stiffness and damping of piles. Canadian Geotechnical Journal 11 (4), 574–598.

Novak M. 1977. Vertical vibration of floating piles. Journal of Engineering Mechanics Division 103 (1), 153–168.

Novak, M., Nogami, T., 1977. Soil-pile interaction in horizontal vibration. Earthquake Engineering and Structural Dynamics 263, 281–285.

Novak M., Sheta M. 1980. Approximate approach to contact effects of piles. Proceedings of Dynamic Response of Pile Found: Analytical aspects ASCE New York, NY 53–79.

Novak, M., Nogami, T., Aboul-ella, F., 1978. Dynamic soil reactions for plane strain case. Journal of Mechanical Engineering Division ASCE 104, 953 959.

Poskitt, T.J., 1991. Energy loses in pile driving due to soil rate effects and hammer misalignment. Proceedings Institution of Civil Engineers 823, 851–891.

Poskitt T.J. 1992. Keynote lecture: problems of reconciling stress wave measurements with theory. Proceedings of the fourth international conference on the application of stress wave theory to piles A.A BALKEMA, Rotterdam, Netherlands, pp 495–507.

Richart, F.E., Wylie, E.B., 1978. Field and laboratory measurements of dynamic soil properties, Dynamical Methods in Soil and Rock Mechanics 1. A. A. Balkema, Rotterdam 3–36.

Richart, F.E., Hall, J.R., Woods, R.D., 1970. Vibration of Soil Foundations. Prentice Hall, Englewood Cliffs, New Jersey.

Seed H., Idriss I.M. 1970. Soil Moduli and Damping Factor for Dynamic Response Analyses Report N° EERC 70-10 University of California Berkley.

Tsuha C.H.C., Foray P.Y., Jardine R.J., Yang Z.X., Silva M., Rimoy S. 2012. Behaviour of displacement piles in sand under cyclic axial loading. Soils and Foundations 52 (3), 393–410.

Vrettos C., Borchrt K.-M. 2011. Combined foundation of a high-rise building complex on sand: Analysis and observation. Soils and Foundations 51 (2), 343–350.

Vucetic, M., Dobry, R., 1991. Effect of soil plasticity on cyclic response. Journal of Geotechnical Engineering ASCE 89, 107–111.

Woods, R.D., Wylie, E.B., 1978. Parameters affecting elastic properties. ic soil properties. Dynamical methods in soil and rock mechanics 1. A. A. Balkema, Rotterdam 37–59.